Brazilian Journal
of Chemical
Engineering

ISSN 0104-6632
Printed in Brazil
www.abeq.org.br/bjche

Vol. 32, No. 01, pp. 269 - 281, January - March, 2015
dx.doi.org/10.1590/0104-6632.20150321s00001715

ADSORPTION OF THE DYE REACTIVE BLUE 5G IN RETORTED SHALE

R. Lambrecht[1], M. A. S. D. de Barros[1], P. A. Arroyo[1], C. E. Borba[2*] and E. A. da Silva[2]

[1]Chemical Engineering Department, State University of Maringá, Av. Colombo 5790,
CEP: 87020-900, Maringá - PR, Brazil.
Phone: + (55) (45) 3379 7092; Fax: + (55) (45) 3379 7000
E-mail: borba_deq@yahoo.com.br
[2] Chemical Engineering Department, State University of the West of Paraná,
Faculty Street 645, La Salle Garden, CEP: 85903-000, Toledo - PR, Brazil.

(Submitted: February 21, 2012 ; Revised: March 19, 2014 ; Accepted: March 21, 2014)

Abstract - In this study the influence of the volumetric flow rate and feed concentration was investigated for the adsorption of the reactive dye Blue 5G. Experiments were carried out in a bed packed with retorted shale, at 30 ^{o}C. The ranges investigated were flow rate 2 -10 mL/min and the feed concentration 13-105 mg/L. Mathematical models were used to represent the dynamic sorption. The double resistance model considers the effects of the axial dispersion and the mass transfer resistance of the external film and inside the particles. As a result, the mass transfer coefficient of the external film and the internal mass transfer coefficient were estimated. The Thomas model was used to simulate the experimental data. In this model the fitted parameter was the adsorption kinetic constant. The first model provided an acceptable representation of the dynamic uptake of the reactive dye Blue 5G.
Keywords: Mathematical modeling; Packed bed; Reactive dye; Adsorption; Shale.

INTRODUCTION

The contamination of natural waters is one of the greatest problems confronting contemporary society. The textile industry is notable among the industries that produce effluents with high pollution loads, commonly composed of organic molecules and complex salts (Koyuncu and Topacik, 2003). The environmental problems caused by dyeing effluents are even more serious when unfixed or non-degraded dyes from conventional treatment processes are discharged, since they have a potentially high environmental impact on water bodies due to their toxicity (Maurya *et al*., 2006).

There are around 10,000 different industrial dyes and pigments, totaling an annual world consumption of 700,000 tons (Pearce *et al*., 2003), 26,500 tons of which are consumed in Brazil (Guaratini and Zanoni, 2000). Reactive Blue 5G is one of the main dyes used in dyeing facilities since it is used in the production of blue denim.

The environmental problems related to the textile industry are numerous and well documented (Mahmoodi *et al*., 2010a; Mahmoodi *et al*., 2010b; Gottipati and Mishra, 2010; Lima *et al*., 2007; Epolito *et al*., 2005). Besides the removal of organic loads, blue color removal is one of the main objectives in the treatment of textile effluents.

Due to the environmental effects of these textile effluent compounds, new technologies for their degradation and immobilization have been investigated. Several physicochemical and biological processes

*To whom correspondence should be addressed

have been used to remove dyes such as Reactive Blue 5G and other compounds from effluents. The physicochemical processes include chemical oxidation (with chlorine, peroxide, or ozone), coagulation, flocculation, precipitation, membranes, ion exchange, and adsorption (Dizge *et al*., 2008).

The process of adsorption in activated carbon-packed beds is an effective method of decolorization (Rozzi *et al*., 1999; Jain and Sikarwar, 2009). In fact, this dynamic process has been widely used as it combines advantages such as reduced space, simple operation, treatment of large volumes of effluent, significant yield, large range of feed concentrations and easy scaling-up (Valdman *et al*., 2001; Silva *et al.*, 2002). Besides studying activated carbon-packed beds, research has also been focused on investigating the use of residues as alternative sorbents, seeking to reduce both the sorbent production and disposal costs. Alternative sorbents include sawdust, fruit bagasse, eucalyptus bark, and chitosan (Crini, 2005), as well as retorted shale, which is produced from burning shale (bituminous rock) in the absence of the oxygen (Lee, 1991). Shale sub-products have been investigated, although scarcely, and the promising use of these materials for the removal of organic molecules has been reported (Tütem *et al.*, 1998; Al-Qodah, 2000).

The design of retorted shale-packed beds requires information on the removal capacity of the sorbent and the mass transfer effects, which are evaluated through the breakthrough curves. The breakthrough curves are influenced by the equilibrium conditions and several other parameters, mainly temperature, volumetric flow rate and particle diameter (Koprivanac *et al*., 2005).

One of the requirements in scaling-up packed beds is a mathematical model that accurately represents the experimental data. Several mathematical models have been successfully used to represent the dynamic dye uptake and these include the Bohart and Adams, Thomas, and Yoon-Nelson models (Rozada *et al*., 2003; Lin *et al*., 2004; Ahmad and Hameed, 2010). Although the good performance of shale oil ash as a dye adsorbent has been successfully predicted through the BDST (Bed Depth Service Time) model (Al-Qodah and Lafi, 2003), few results which take into account the mass transfer mechanism have been reported. Therefore, the main objective of this study was to evaluate a mathematical model that represents the adsorption of Reactive Blue 5G in retorted shale. The mathematical model investigated considered the intraparticle and film mass transfer. The influence of volumetric flow and feed concentration on the sorption mechanism was investigated and the accuracy of the model is discussed.

MATERIAL AND METHODS

Adsorbent

All experiments were carried out using a Petrosix (a Petrobras subsidiary) retorted shale sample. The sample was also submitted to a sieving classification.

Reactive Blue 5G Dye

Dye solutions were prepared with a commercial sample manufactured by Texpal Química Industry. The concentration of dye in each solution (13-105 mg/L) was determined by UV/Vis spectroscopy in the 350-1000 nm wavelength range on a Shimadzu UV-Visible spectrophotometer (UV - 1601PC) at 610 nm, which was experimentally determined. This wavelength is in agreement with results reported in Batzias and Sidiras (2004).

Fixed-Bed Column Assays

The adsorption unit is shown in Figure 1. The module consisted of a stock solution reservoir and a deionized water reservoir, which was used to homogenize the bed and stabilize the flow rate. A Cole Parmer peristaltic pump fed the column (ID of 1.01 cm) that contained the packed bed and was kept at a constant temperature of 30 ^{o}C. Runs were carried out using an up-flow process and outlet samples were carefully taken at regular running times. Analysis of the dye concentration of each sample allowed the plotting of the breakthrough (C/C_0 *versus* time) curves.

Five runs with a feed concentration of 35 mg/L were carried out using different flow rates (2.0; 4.0; 6.0; 8.0 and 10.0 mL/min) at 30 ^{o}C. In each run performed the inlet solution percolated a packed bed of 7.264 g of retorted shale. The total packed bed height (L) was 9.5 cm. From the breakthrough curves obtained it was possible to determine the flow rate that minimized the mass transfer resistances.

After the best operational conditions had been established, ten more runs were carried out with different feed concentrations (13.32, 22.08, 35.03, 40.69, 46.37, 52.61, 54.86, 68.78, 84.72 and 104.97 mg/L).

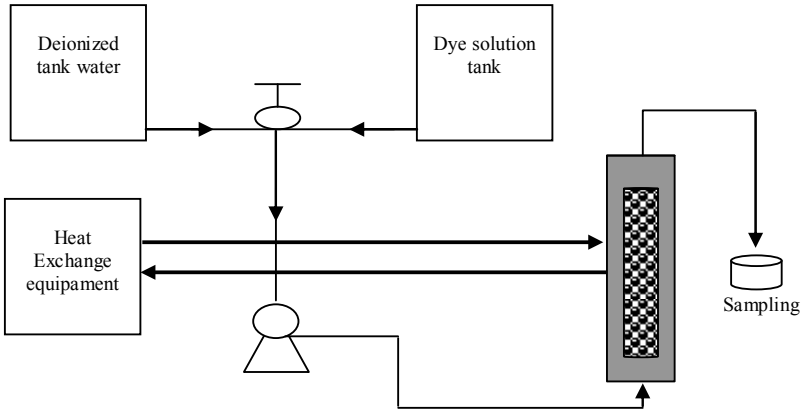

Figure 1: Scheme of the experimental module.

Calculation of the Column Adsorption Capacity and the Length Of Unused Bed (LUB)

The amount of dye removed by the adsorbent was calculated from experimental breakthrough curves using the mass balance:

$$q^* = \frac{\dot{Q} C_0}{m_s} \int_0^t \left(1 - \frac{C_{out}}{C_0}\right) dt - \frac{V_L \varepsilon C_0}{m} \quad (1)$$

where q^* is the amount of dye which has been removed when equilibrium is reached (mg/g), $\dot{Q}$ is the volumetric flow (L/min), C_0 is the feed concentration, m_s is the mass of adsorbent, C_{out} is the dye concentration at the column outlet, V_L is the bed volume and ε is the bed porosity. The bed porosity was determined as methodology presented by Borba *et al*. (2006).

The integral in Equation (1) was solved numerically by the trapezoid rule, using the experimental data obtained from the breakthrough curves.

A plot of q^* against C_0 for the ten experimental runs using different feed concentrations generated the dynamic isotherm (isotherms obtained through breakthrough data – Ernest Jr., 1997; Gazola *et al*., 2006). The Langmuir parameters were then estimated through a nonlinear fitting method (Ostroski *et al*.; 2009).

When a favorable isotherm is observed, the concentration profile in the mass- transfer zone acquires a wave shape that does not change as the zone moves through the bed. The *LUB* is obtained as related in Geankoplis (2003).

MATHEMATICAL MODELING

In this study, the process of dye removal in a packed bed filled with retorted shale was modeled through two models. The first one assumes that the adsorption process can be described by a pseudo second-order rate expression and was developed by Thomas (1944). The second model assumes internal and external mass transfer limitations. Both models consider the following assumptions related to the operating conditions: constant column void fraction, constant physical properties of the solid and fluid phases, and isothermal and isobaric process conditions.

Thomas Model

The Thomas model considers the following assumptions: axial and radial dispersion in the packed bed column is negligible, the adsorption rate is described by Langmuir kinetics and intraparticle diffusion and external resistances are negligible.

On the basis of these assumptions, the mass balance of the dye concentration in the fluid phase is described by:

$$\frac{\partial C(z,t)}{\partial t} + \frac{\rho_B}{\varepsilon} \frac{\partial \overline{q}(z,t)}{\partial t} + u_0 \frac{\partial C(z,t)}{\partial z} = 0 \quad (2)$$

where C is the concentration of dye in the bulk liquid phase (mg/L), $\overline{q}$ is the average concentration of the dye in the adsorbent (mg/g), ρ_B is the density of the bed (g/L), ε is the porosity of the bed, t is the time (min) and z is the bed height (cm).

The Thomas model assumes that the adsorption

process can be described by a pseudo second-order rate expression given by:

$$\frac{\partial \overline{q}(z,t)}{\partial t} = k_a\left(q_{\max} - \overline{q}(z,t)\right)C(z,t) - k_d\overline{q}(z,t) \quad (3)$$

where k_a is the adsorption kinetic constant (L /mg min), k_d stands for the desorption kinetic constant (min^{-1}) and $q_{\max}$ is the maximum adsorption capacity (mg/g).

At equilibrium, $\partial\overline{q} / \partial t = 0$ and Eq. (3) is simplified to give the Langmuir isotherm:

$$\overline{q} = q^* = \frac{q_{\max} b C^*}{1 + bC^*} \quad (4)$$

where $q_{\max}$ is the Langmuir isotherm parameter for the maximum adsorption capacity (mg/g), b is the Langmuir equilibrium constant parameter isotherm (L/mg) and $C = C^*$ at equilibrium.

The Langmuir constant can be defined as the ratio between the adsorption and desorption rate constants ($b = k_a/k_d$). Hence, Eq. (3) can be rewritten as follows:

$$\frac{\partial \overline{q}(z,t)}{\partial t} = k_a\left(q_{\max} - \overline{q}(z,t)\right)C(z,t) - \frac{k_a}{b}\overline{q}(z,t) \quad (5)$$

The initial conditions of the fluid phase concentration and of the average concentration of adsorbed dye in the solid phase are, respectively:

$$C(z,0) = 0 \quad (6)$$

$$\overline{q}(z,0) = 0 \quad (7)$$

The boundary condition suggested by Amundson (1948) are:

$$C(0,t) = \begin{cases} 0 & t = 0 \\ C_0 & t > 0 \end{cases} \quad (8)$$

The analytical solution to the Thomas model is obtained after solving Equations (2) and (3) with the initial conditions provided by Eqs. (6)-(7) and the boundary conditionsof Eq. (8), as reported elsewhere (Thomas, 1944; Borba *et al*., 2008).

The parameter k_a of the Thomas model was obtained by fitting the experimental breakthrough data using UVMIF in the Fortran IMSL subroutines Therefore, k_a is obtained through the minimization of the objective function:

$$F_{OBJ} = \sum_{i=1}^{n}\left(\frac{C\Big|_{z=L}^{\exp}}{C_0} - \frac{C\Big|_{z=L}^{\mathrm{mod}}}{C_0}\right)^2 \quad (9)$$

where n is the number of experimental data points, $C\Big|_{z=L}^{\exp}$ is the experimental dye concentration when $z = L$ and $C\Big|_{z=L}^{\mathrm{mod}}$ is the dye concentration, calculated by the model, when $z = L$.

Double Resistance Model

In this study, a more realistic model that considers double limitation effects was applied to describe the dynamic removal of dye in the packed bed. The main assumptions in the mathematical modeling of the adsorption of the reactive dye in the packed bed were: solid/fluid interface equilibrium can be represented by the Langmuir isotherm, external film and intraparticle mass transfers occur and a linear driving force describes the concentration profile inside the particles.

Based on the above-mentioned assumptions, the mass balance of the dye in the fluid phase can be described by:

$$\frac{\partial C(z,t)}{\partial t} + u_0\frac{\partial C(z,t)}{\partial z} + \rho_B\frac{1}{\varepsilon}\frac{\partial \overline{q}(z,t)}{\partial t} - D_L\frac{\partial^2 C(z,t)}{\partial z^2} = 0 \quad (10)$$

where D_L is the axial dispersion coefficient in the liquid phase (cm^2/min).

The mass transfer equations for the dye concentration in the external liquid film and for dye adsorption onto the solid particles are, respectively:

$$\frac{\partial \overline{q}(z,t)}{\partial t} = \frac{K_F\,\varepsilon}{\rho_B}\left(C(z,t) - C^*\right) \quad (11)$$

$$\frac{\partial \overline{q}(z,t)}{\partial t} = -K_S\left(\overline{q}(z,t) - q^*\right) \quad (12)$$

where K_F is the mass transfer volumetric coefficient in the external liquid film (min^{-1}), K_S is the volumetric mass transfer coefficient of the adsorbent (min^{-1}), C^* is the dye concentration in the liquid phase at equilibrium (mg/L) and q^* is the dye concentration on the adsorbent at equilibrium (mg/g).

Equation (12) considers that the mass transfer driving force varies linearly with the concentration of the dye sorbent. It is an approximation of the Fick law and is called the linear driving force model, which was originally proposed by Glueckauf and Coates (1947). This model has been successfully applied to describe the adsorption of dye (Chuang *et al*., 2003) from aqueous solution and organic components from the gas phase (Dantas *et al*., 2011; Otero *et al*., 2005).

The variables *q** and *C** are related by the Langmuir isotherm. The mathematical expression of the Langmuir isotherm for a monocomponent system is represented by Eq. (4).

The mass transfer volumetric coefficient in the adsorbent (K_S) can be expressed as a function of the local concentration of the dye in the fluid phase (Crank, 1979).

$$K_S = K_{S0}\frac{1}{1+AC_{local}} \tag{13}$$

where C_{local} is the local concentration of the dye in the liquid phase.

The initial conditions of this model are given by Eqs. (6) and (7). The boundary conditions are written as suggested by Danckwerts (1953).

$$D_L\frac{\partial C(z,t)}{\partial z} = u_0\left(C(0,t)-C_0\right) \text{ at } z=0 \tag{14}$$

$$\frac{\partial C(z,t)}{\partial z} = 0 \text{ at } z=L \tag{15}$$

In this study, the double resistance model was used in two different ways. First, the mass transfer coefficient in the solid phase is local-concentration independent. Secondly, the mass transfer coefficient in the solid phase is a function of the local concentration, as described in Eq. (13).

The mathematical models were solved using the finite volume method (Maliska, 1995). The system of partial differential equations was discretized in the axial coordinate *z*. This generated a set of ordinary time differential equations. These equations were solved according to the respective initial conditions by the subroutine DASSL in the Fortran code (Petzold, 1982).

Three groups of parameters are identified in the mathematical models. The first is related to the experimental data. Parameters such as ρ_B, ε and u_0 are examples. The second group includes the parameter D_L, estimated as a function of the empirical equations. Finally, the third group considers some parameters estimated through the non-linear adjustment of the models to the experimental data and the least squares criterion. Parameters such as $q_{\max}$, b, K_F, K_S, K_{S0}, and A are good examples of the third group. More specifically, K_F, K_S, K_{S0} and A were obtained from the experimental data for the breakthrough, whereas $q_{\max}$ and b were calculated from the equilibrium data.

The axial dispersion coefficient was estimated according to (Ruthven, 1984):

$$\frac{D_L}{u_0 d_p} = \frac{20}{\varepsilon}\left(\frac{D_m}{u_0 d_p}\right)+\frac{1}{2} \tag{16}$$

where D_m is the molecular diffusivity of the dye in water (cm^2/min) and d_p the particle diameter of the adsorbent (cm).

Parameter Identification Method

In this study, the model parameters were estimated in the non-linear fitting procedure using the experimental data and least squares statistical method to form the objective function (criterion). The values for the model parameters (K_F, K_S, K_{S0}, A) were obtained during the search for the minimum of the objective function represented by Eq. (9). In the search procedure, the optimization method of Nelder and Mead (1965), in Fortran code, was used.

RESULTS AND DISCUSSION

Adsorbent

Samples used in the sorption process had an average particle diameter of 0.22 mm, according to the sieving procedure.

Dynamic Adsorption

In order to obtain the dynamic isotherm, breakthrough curves at various flow rates were obtained. The saturation points were 1500, 790, 600, 480 and 200 min for the volumetric flows rates of 2, 4, 6, 8 and 10 mL/min, respectively. The lengths of unused bed (*LUB*) are given in Table 1. It can be seen that the *LUB* increased with the flow rate. When the flow rate increases, the residence time in the bed decreases, which results in lower bed utilization (Ko *et al*., 2001). Consequently, there was not sufficient contact time for the dye to diffuse in the adsorbent. An optimal operational flow rate is assumed to exist for

a specific sorbent/sorbate system in which the residence time is sufficient for the dye uptake without significant external resistance (Geankoplis, 2003). Because the *LUB* was the shortest at 2 mL/min, this was assumed to be the operational condition that best minimized the mass transfer resistances.

Table 1: *LUB* as a function of flow rate. T = 30 °C, m_{ads} = 7.264 g.

Q (mL min^{-1})	*LUB* (cm)
2.00	4.27
4.00	5.91
6.00	5.87
8.00	6.53
10.00	6.49

The experimental equilibrium data for the dye adsorption and the Langmuir isotherm models are shown in Figure 2. The values for the fitted parameters of the Langmuir model were: q_{max} = 2.955 mg/g and b = 0.146 L/mg. The average deviation between the experimental and calculated data for the dye uptake capacity was 3.59% and the determination coefficient was 0.9840. Since this coefficient is close to unity, it indicates a good fit between the model and the experimental data.

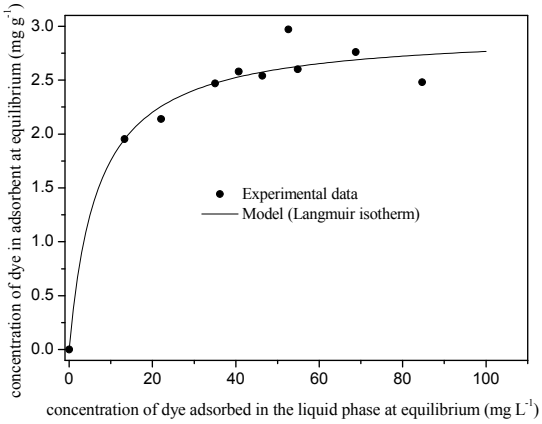

Figure 2: Isotherm of dye adsorption on retorted shale – Experimental data and Langmuir Model. T = 30 °C, m_{ads} = 7.264 g, Q = 2 mL min^{-1}.

Modeling of the Breakthrough Curves- Effect of Volumetric Flow Rate

As expected, an increase in the flow rate resulted in a shorter time being required to reach the breakpoint. Moreover, when the flow rate was higher, the breakthrough curve was steeper. This effect can be observed in Figure 3.

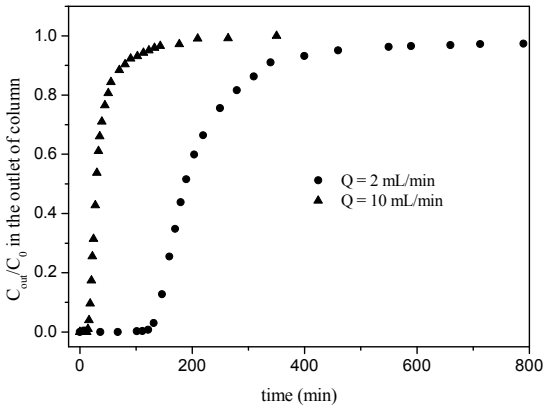

Figure 3: Effect of flow rate on the breakthrough curve. T = 30 °C, m_{ads} = 7.264 g, (●) 2 mL min^{-1}, (▲) 10 mL min^{-1}.

The packed-bed characteristics necessary for the model applications were: ρ_B = 954.9 g/L, d_L = 1.01 cm and ε = 0.50. The values for the dispersion coefficients required for the double resistance model were calculated by applying Eq. (21). The molecular diffusion coefficient of the dye in water was $1.33\times10^{-5}\,cm^2/min$. This coefficient was calculated by the Wilke–Chang equation (Miyabe and Isogai, 2011). The values for the axial dispersion coefficients are presented in Table 2.

Table 2: Axial dispersion coefficient calculated as a function of the volumetric flow. T = 30 °C, m_{ads} = 7.264g.

Q (mL min^{-1})	D_L (cm^2 min^{-1})
2.00	0.53
4.00	1.06
6.00	1.60
8.00	2.09
10.00	2.59

Table 3 presents the fitted parameters of the Thomas and double resistance models in which the volumetric mass transfer coefficient is expressed as a constant in the solid phase and as a function of the local concentration of the dye in the liquid phase.

The values of the objective function and the determination coefficient for each experimental condition are presented in Table 4. The low values for the objective function and the high values for the determination coefficient of the double resistance model, with variable K_S as a function of the local concentration of the dye in the liquid phase, best fitted the experimental breakthrough curves. This can be observed in Figures 4-8, which show the results for the experimental breakthrough data and the curves simulated by the models.

Table 3: Effect of the flow rate in the fitted parameters of the models (T = 30 °C, m_{ads} = 7.264 g).

Q (mL min^{-1})	C_0 (mg L^{-1})	Model parameters with constant K_S		Model parameters with variable K_S			Thomas Model parameters
		K_S (min^{-1})	K_F (min^{-1})	K_{S0} (min^{-1})	A	K_F (min^{-1})	k_a (L mg^{-1} min^{-1})
2.00	34.26	10.94 x 10^{-3}	2.74 x 10^{5}	15.95	72.71	754.00	4.38 x 10^{-4}
4.00	35.06	14.00 x 10^{-3}	2.56 x 10^{5}	16.69	78.13	782.80	6.33 x 10^{-4}
6.00	34.03	19.57 x 10^{-3}	5.61 x 10^{5}	17.03	77.73	876.20	1.11 x 10^{-3}
8.00	34.73	21.64 x 10^{-3}	5.30 x 10^{5}	16.95	72.73	1013.20	1.41 x 10^{-3}
10.00	34.67	33.85 x 10^{-3}	2.35 x 10^{5}	15.52	69.21	1169.80	1.68 x 10^{-4}

Table 4: Effect of the flow rate in the objective function and coefficient of determination values (T =30 °C, m_{ads} = 7.264 g).

Q (mL min^{-1})	Model with constant K_S		Model with variable K_S		Thomas Model	
	F_{OBJ}	r^2	F_{OBJ}	r^2	F_{OBJ}	r^2
2.00	0.1698	0.9218	0.0299	0.9835	0.4589	0.8546
4.00	0.3085	0.8935	0.0952	0.9728	0.5573	0.8030
6.00	0.3380	0.8892	0.0985	0.9736	0.5514	0.8065
8.00	0.4697	0.8312	0.1476	0.9572	0.6479	0.7851
10.00	0.3486	0.8788	0.0906	0.9792	3.7610	0.5215

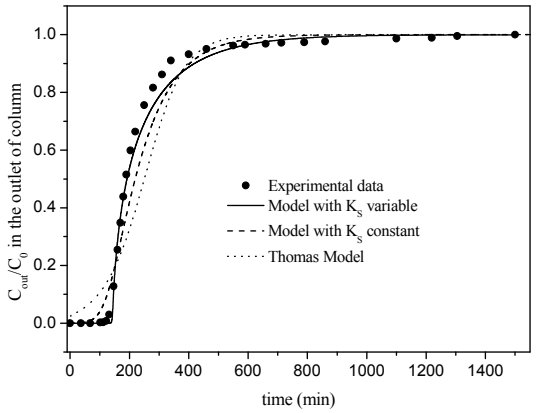

Figure 4: Experimental and calculated breakthrough curves. T = 30 °C, m_{ads} = 7.264 g, Q = 2 mL min^{-1}.

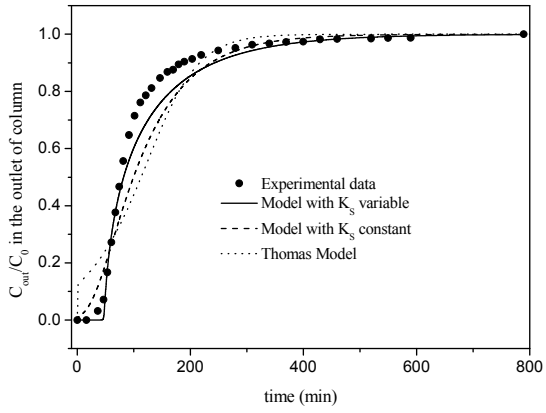

Figure 5: Experimental and calculated breakthrough curves. T = 30 °C, m_{ads} = 7.264 g, Q = 4 mL min^{-1}.

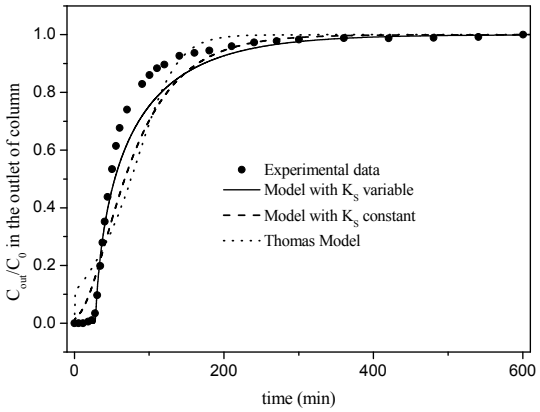

Figure 6: Experimental and calculated breakthrough curves for T = 30 °C, m_{ads} = 7.264 g, Q = 6 mL min^{-1}.

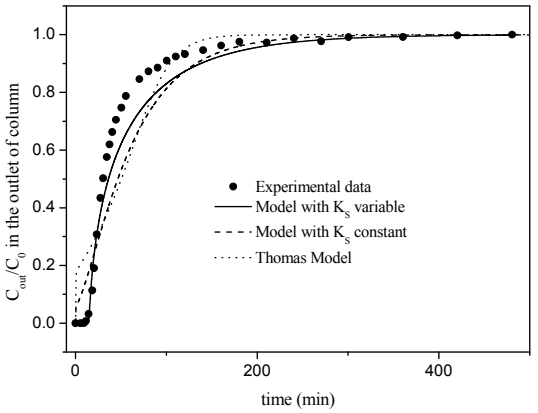

Figure 7: Experimental and calculated breakthrough curves for T = 30 °C, m_{ads} = 7.264 g, Q = 8 mL min^{-1}.

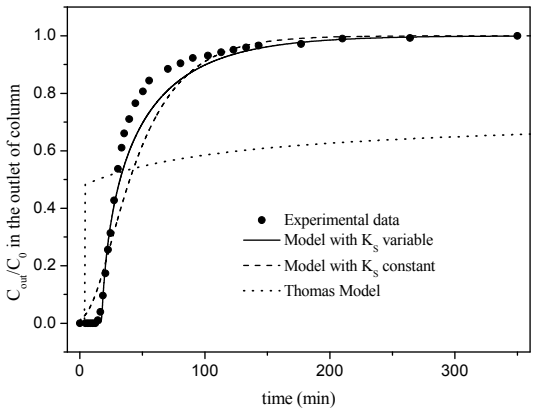

Figure 8: Experimental and calculated breakthrough curves for T = 30 °C, m_{ads} = 7.264 g, Q = 10 mL min^{-1}.

Changes in the double resistance model with variable K_S were as expected and the values are given in Table 4. The values for the parameter K_F increased with increasing flow rates, while K_S is flow-rate independent.

Effect of Feed Concentration

As expected, an increase in the feed concentration resulted in a shorter time being required to reach the breakpoint, indicating a lower treated volume. Moreover, when the feed concentration was higher, the breakthrough curve was steeper, as a consequence of a higher mass transfer between the fluid and solid phases. This effect can be observed in Figure 9.

The experimental and simulated results for the breakthrough data for different feed concentrations are shown in Figures 10-19. The values for the fitted parameters are given in Table 5. The values of the objective function and determination coefficient, for each experimental condition analyzed are presented in Table 6. It can be observed that the values for the double resistance model with variable K_S showed the best fit for the experimental breakthrough data. Also, the changes in the numerical values of variable K_S when the double resistance model was considered were as expected.

It was noted that K_S increased with increasing feed concentration, while the K_F values were feed-concentration independent. According to Ko *et al*. (2001), the driving force for the mass transfer in the adsorption is determined by the differences in the local concentration between the phases. This explains the better performance of the model when the mass transfer coefficient for the adsorbent was considered to be function of the local concentration of the dye in the liquid phase.

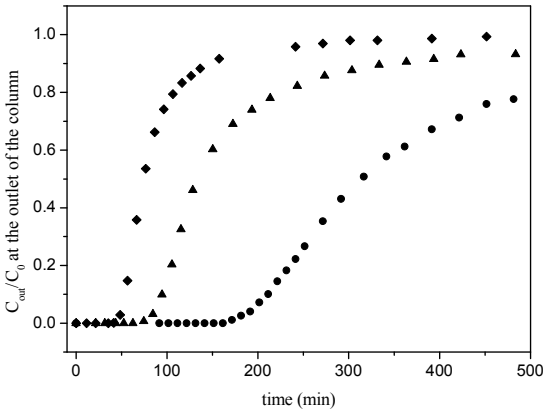

Figure 9: Effect of feed concentration on the breakthrough curve. T = 30 °C, m_{ads} = 7.264 g, (♦) C_0 = 13.32 mg L^{-1}, (▲) C_0 = 52.61 mg L^{-1}, (●) C_0 = 104.91 mg L^{-1}.

Table 5: Effect of the feed concentration in the fitted parameters of the models (T = 30 °C, m_{ads} = 7.264 g).

C_0 (mg L^{-1})	Q (mL min^{-1})	Model parameters with constant K_S		Model parameters with variable K_S			Thomas Model parameters
		K_S (min^{-1})	K_F (min^{-1})	K_{S0} (min^{-1})	A	K_F (min^{-1})	k_a (L mg^{-1} min^{-1})
13.32	2.00	4.90 x 10^{-3}	1.49 x 10^{4}	8.64	241.17	718.55	3.68 x 10^{-4}
22.08		5.22 x 10^{-3}	5.00 x 10^{3}	11.07	159.87	771.08	2.65 x 10^{-4}
35.03		9.70 x 10^{-3}	3.38 x 10^{3}	14.71	78.48	814.58	4.19 x 10^{-4}
40.69		10.00 x 10^{-3}	1.47 x 10^{4}	16.81	70.34	768.38	3.51 x 10^{-4}
46.37		10.86 x 10^{-3}	9.34 x 10^{3}	18.64	63.52	760.30	3.17 x 10^{-4}
52.61		13.78 x 10^{-3}	1.32 x 10^{3}	22.41	51.06	730.20	4.27 x 10^{-4}
54.86		11.52 x 10^{-3}	2.90 x 10^{3}	21.08	54.15	779.60	2.69 x 10^{-4}
68.78		16.96 x 10^{-3}	1.30 x 10^{4}	26.26	36.68	806.20	4.03 x 10^{-4}
84.72		17.48 x 10^{-3}	8.54 x 10^{3}	28.95	31.21	761.80	3.57 x 10^{-4}
104.97		26.03 x 10^{-3}	1.34 x 10^{3}	34.67	22.55	802.10	4.57 X 10^{-4}

Table 6: Effect of the feed concentration in the objective function and coefficient of determination values (T = 30 °C, m_{ads} = 7.264 g).

C_0 (mg L^{-1})	Model with constant K_S		Model with variable K_S		Thomas Model	
	F_{OBJ}	r^2	F_{OBJ}	r^2	F_{OBJ}	r^2
13.32	0.5724	0.8061	0.1362	0.9591	0.1101	0.9645
22.08	0.3713	0.8592	0.0690	0.9612	0.8712	0.8007
35.03	0.1924	0.9156	0.0206	0.9856	0.5100	0.8174
40.69	0.2751	0.8978	0.0333	0.9733	0.6516	0.7974
46.37	0.2376	0.9011	0.0328	0.9773	0.5421	0.8378
52.61	0.0660	0.9703	0.0310	0.9789	0.2399	0.9132
54.86	0.2264	0.9017	0.0289	0.9809	0.5095	0.8232
68.78	0.0687	0.9654	0.0074	0.9905	0.2764	0.8915
84.72	0.1283	0.9623	0.0334	0.9725	0.4381	0.8367
104.97	0.0391	0.9862	0.0136	0.9845	0.2101	0.9023

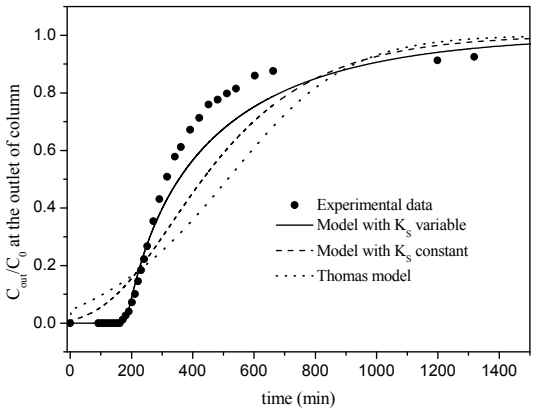

Figure 10: Experimental and calculated break-through curves. T = 30 °C, m_{ads} = 7.264 g and C_0 = 13.32 mg L^{-1}.

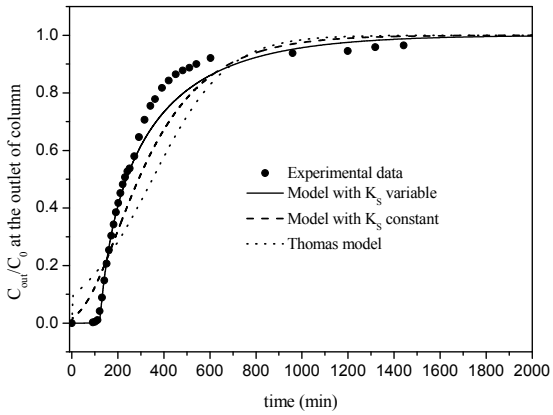

Figure 11: Experimental and calculated break-through curves. T = 30 °C, m_{ads} = 7.264 g and C_0 = 22.08 mg L^{-1}.

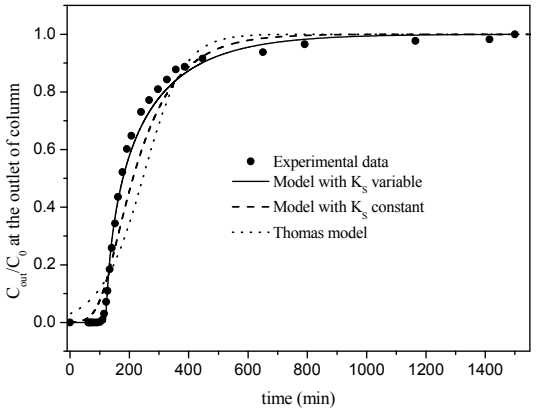

Figure 12: Experimental and calculated breakthrough curves. T = 30 °C, m_{ads} = 7.264 g and C_0 = 35.03 mg L^{-1}.

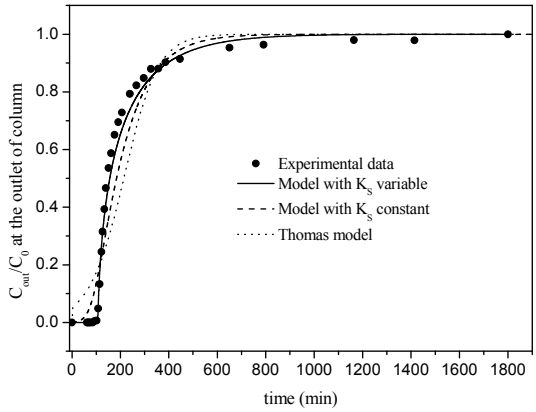

Figure 13: Experimental and calculated breakthrough curves. T = 30 °C, m_{ads} = 7.264 g and C_0 = 40.69 mg L^{-1}.

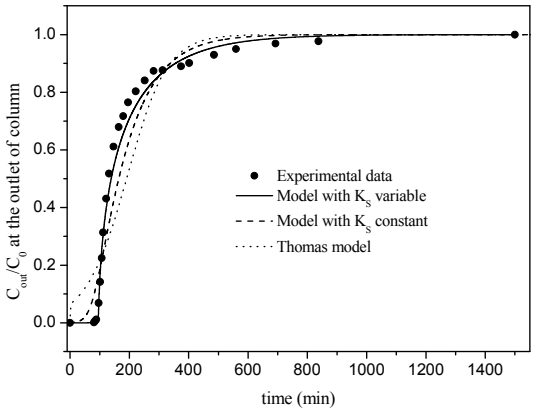

Figure 14: Experimental and calculated breakthrough curves. T = 30 °C, m_{ads} = 7.264 g and C_0 = 46.37 mg L^{-1}.

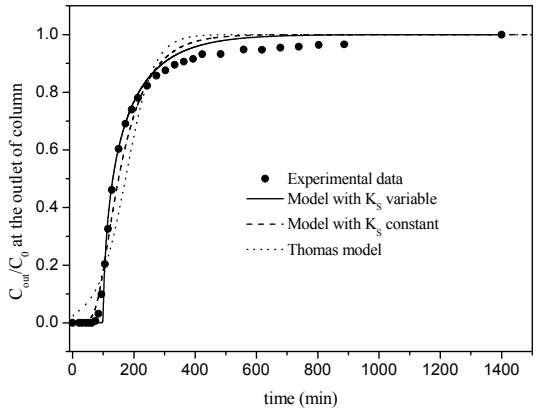

Figure 15: Experimental and calculated breakthrough curves. T = 30 °C, m_{ads} = 7.264 g and C_0 = 52.61 mg L^{-1}.

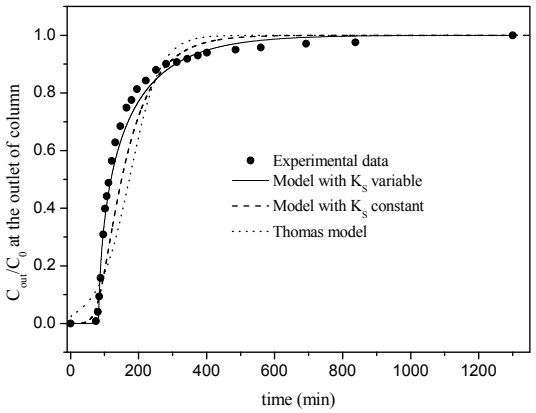

Figure 16: Experimental and calculated breakthrough curves. T = 30 °C, m_{ads} = 7.264 g and C_0 = 54.86 mg L^{-1}.

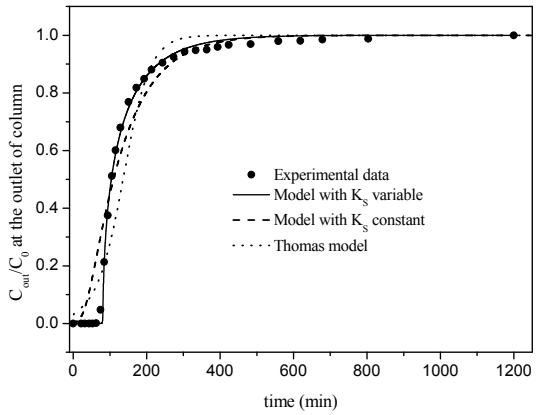

Figure 17: Experimental and calculated breakthrough curves. T = 30 °C, m_{ads} = 7.264 g and C_0 = 68.78 mg L^{-1}.

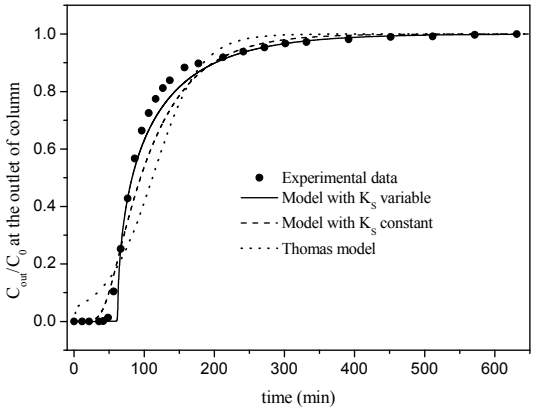

Figure 18: Experimental and calculated breakthrough curves. T = 30 °C, m_{ads} = 7.264 g and C_0 = 84.72 mg L^{-1}.

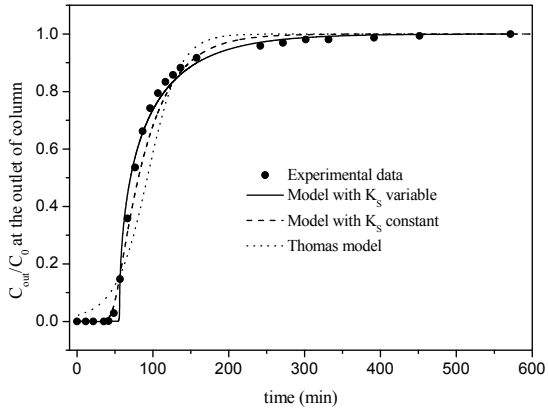

Figure 19: Experimental and calculated breakthrough curves. T = 30 °C, m_{ads} = 7.264 g and C_0 = 104.97 mg L^{-1}.

CONCLUSIONS

In this study the adsorption of Reactive Blue 5G on a packed bed was investigated using retorted shale as the adsorbent. The Langmuir isotherm model adequately described the experimental equilibrium data. The dye adsorption process was influenced by the volumetric flow rate, as well as by the feed concentration. It was concluded that 2 mL/min was the best flow rate as it minimizes the mass transfer resistances. An increase in feed concentration decreased the mass transfer resistance because it provided a greater driving force.

Based on the simulation results it can be concluded that the double resistance model with at solid mass transfer coefficient that is a function of the local concentration of the dye in the liquid phase best represented the dynamic dye adsorption. In addition, the model appears to be a very useful tool for phenomenological studies as well as for process optimization and packed bed design of the system studied herein.

NOMENCLATURE

A	fitted parameter of Eq. (15)	L mg^{-1}
b	Langmuir isotherm parameter	L mg^{-1}
C	concentration of dye in the bulk liquid phase	mg L^{-1}
C_0	concentration of dye in the feed	mg L^{-1}
C_{out}	concentration of dye at the column outlet	mg L^{-1}
C_{local}	local concentration of the dye in the liquid phase	mg L^{-1}
C^*	concentration of dye in the liquid phase at equilibrium	mg L^{-1}
D_L	axial dispersion coefficient in the liquid phase	cm^2 min^{-1}
D_m	molecular diffusivity of the dye in water	cm^2 min^{-1}
d_p	particle diameter of the adsorbent	cm
H_t	total bed height	cm
k_a	adsorption rate constant	L mg^{-1} min^{-1}
k_d	Desorption rate constant	min^{-1}
K_F	volumetric mass transfer coefficient in the external liquid film	min^{-1}
K_S	volumetric mass transfer coefficient of the adsorbent	min^{-1}
K_{S0}	volumetric mass transfer coefficient of the adsorbent	min^{-1}
m_s	mass of adsorbent	g
$\overline{q}$	average concentration of the dye in the adsorbent	mg g^{-1}
q_b	amount of dye which has been removed when the breakthrough point is reached	mg g^{-1}
q_{max}	maximum adsorption capacity (Langmuir isotherm parameter)	mg g^{-1}
q^*	amount of dye which has been removed when equilibrium is reached	mg g^{-1}
$\dot{Q}$	volumetric flow	mL min^{-1}

u_0	interstitial velocity	cm min^{-1}
t	time coordinate	min
t_b	breakthrough time	min
z	space coordinate	cm

Greek Letters

ε	porosity of the bed	
ρ_B	density of the bed	g L^{-1}

REFERENCES

Ahmad, A. A., Hameed, B. H., Fixed-bed adsorption of reactive azo dye onto granular activated carbon prepared from waste. Journal of Hazardous Materials, v. 175, 298-303 (2010).

Al-Qodah, Z., Adsorption of dyes using shale oil ash. Water Research, v. 17, 4295-4303 (2000).

Al-Qodah, Z., Lafi, W., Adsorption of reactive dyes using shale oil ash in fixed beds. Journal of Water of Supply: Research and Technology-AQUA, v. 52, 189-198 (2003).

Amundson, N. R., A note on the mathematics of adsorption in beds. Journal of Physical and Colloid Chemistry, v. 52, 1153-1157 (1948).

Batzias, F. A., Sidiras, D. K., Dye adsorption by calcium chloride treated beech sawdust in batch and fixed-bed systems. Journal of Hazardous Materials, 114, 167-174 (2004).

Borba, C. E., Guirardello, R., Silva, E. A., Veit, M. T., Tavares, C. R. G., Removal of nickel(II) ions from aqueous solution by biosorption in a fixed bed column: Experimental and theoretical breakthrough curves. Biochemical Engineering Journal, 30, 184-191 (2006).

Borba, C. E., Silva, E. A., Fagundes-Klen, M. R., Kroumov, A. D., Guirardello, R., Prediction of the copper (II) ions dynamic removal from a medium by using mathematical models with analytical solution. Journal of Hazardous Materials, v. 152, 366-372 (2008).

Chuang, C. L., Chiang, P. C., Chang, E. E., Modeling VOCs adsorption onto activated carbon. Chemosphere, v. 53, 17-27 (2003).

Crank, J., The Mathematics of Diffusion. Clarendon Press, Oxford (1975).

Crini, G., Non-conventional low-cost adsorbents for dye removal: A review. Bioresource Techonology, v. 97, 1061-1085 (2005).

Danckwerts, P. V., Continuos flow systems: Distribution of residence times. Chemical Engineering Science, v. 2, 1-13 (1953).

Dantas, T. L. P., Luna, F. M. T., Silva Jr., I. J., Torres, A. E. B., de Azevedo, D. C. S., Rodrigues, A. E., Moreira, R. F. P. M., Modeling of the fixed-bed adsorption of carbon dioxide and a carbon dioxide-nitrogen mixture on zeolite 13X. Brazilian Journal of Chemical Engineering, v. 28(3), 533-544 (2011).

Dizge, N., Aydiner, C., Demirbas, E., Kobya, M., Kara, S., Adsorption of reactive dyes from aqueous solutions by fly ash: Kinetic and equilibrium studies. Journal of Hazardous Materials, v. 150, 737-746 (2008).

Ernest Jr., M. V., Whitely, R. D., Ma, Z., Linda Wang, N. H., Effects of mass action equilibria on fixed-bed multicomponent ion-exchange dynamics. Ind. Eng. Chem. Res., v. 36, 212-226 (1997).

Epolito, W. J., Lee, Y. H., Bottomley, L. A., Pavlostathis, S. G., Characterization of the textile anthraquinone dye Reactive Blue 4. Dyes and Pigments, v. 67, 35-46, (2005).

Gazola, F. C. Pereira, M. R., Barros, M. A. S. D., Silva, E. A., Arroyo, P. A., Removal of Cr^{3+} in fixed bed using zeolite NaY. Chemical Engineering Journal, v. 117, 253-261 (2006).

Geankoplis, C. J., Transport Process and Unit Operations. PTR Prentice Hall, USA (1993).

Gottipati, R., Mishra, S., Application of biowaste (waste generated in biodiesel plant) as an adsorbent for the removal of hazardous dye – methylene blue – from aqueous phase. Brazilian Journal of Chemical Engineering, v. 27(2), 357-367 (2010).

Glueckauf, E., Coates, J. J., Theory of chromatography part IV: The influence of incomplete equilibrium on the front boundary of chromatograms and on the effectiveness of separation. Journal of American Chemical Society, 1315-1321 (1947).

Guaratini, C. C. I., Zanoni, M. V. B., Dye textile. New Chemical, v. 23, 1-21 (2000).

Jain, R., Sikarwar, S., Adsorptive removal of Erythrosine dye onto activated low cost de-oiled mustard. Journal of Hazardous Materials, v. 164, 627-633 (2009).

Ko, D. C. K., Porter, J. F., Mckay, G., Film-pore diffusion model for the fixed-bed sorption of copper and cadmium ions onto bone char. Water Research, v. 35, 3876-3886 (2001).

Koprivanac, N., Kusic, H., Vujevi, D., Peternel, I., Locke, B. R., Influence of iron on degradation of organic dyes in corona. Journal of Hazardous Materials, v. 117, 113-119 (2005).

Koyuncu, I., Topacik, D., Effects of operating conditions on the salt rejection of nanofiltration membranes in reactive dye/salt mixtures. Separation Purification Technology, v. 33, 283-294 (2003).

Lee, S., Oil Shale Technology. CRC Press (1991).

Lima, R. O. A., Bazo, A. P., Salvadori, D. M. F., Rech, C. M., Oliveiram D. P., Umbuzeiro, G. A., Mutagenic and carcinogenic potential of a textile azo dye processing plant effluent that impacts a drinking water source. Mutation Research, v. 626, 53-60 (2007).

Lin, S. H., Juang, R. S., Wang. Y. H, Adsorption of acid dye from water onto pristine and acid-activated clays in fixed beds. Journal of Hazardous Materials, v. 113, 195-200 (2004).

Mahmoodi, N. M., Hayati, B., Arami, M., Textile dye removal from single and ternary systems using date stones: Kinetic, isotherm, and thermodynamic studies. Journal of Chemical Engineering Data, v. 55, 4638-4649 (2010b).

Mahmoodi, N. M., Hayati, B., Arami, M., Mazaheri, F., Single and binary system dye removal from colored textile wastewater by a dendrimer as a polymeric nanoarchitecture: Equilibrium and kinetics. Journal of Chemical Engineering Data, v. 55, 4660-4668 (2010a).

Maliska, C. R., Transferência de Calor e Mecânica dos Fluidos Computacional. Livros Técnicos e Científicos, Editora S. A., Rio de Janeiro (1995). (In Portuguese).

Maurya, N. S., Mittal, A. K., Cornel, P., Rother, E., Biosorption of dyes using dead macro fungi: Effect of dye structure, ionic strength and pH. Bioresource Technology, v. 97, 512-521 (2006).

Miyabe, K., Isogai, R., Estimation of molecular diffusivity in liquid phase systems by the Wilke-Chang equation. Journal of Chromatography A, v. 1218, 6639-6645, 2011.

Nelder, J. A., Mead, A., Simplex method for function minimization. Computer Journal, v. 7, 308-315 (1965).

Ostroski, I. C., Barros, M. A. S. D., Silva, E. A., Dantas, J. H., Arroyo, P. A., Lima, O. C. M., A comparative study for the ion exchange of Fe(III) and Zn(II) on zeolite NaY. Journal of Hazardous Materials, v. 161, 1404-1412 (2009).

Otero, M., Zabkova, M., Rodrigues, A. E., Comparative study of adsorption of phenol and salicylic acid from aqueous solution onto nonionic polymeric resins. Separation and Purification Technology, v. 45, 86-95 (2005).

Pearce, C. I., Lloyd, J. R., Guthrie, J. T., The removal of color from textile wastewater using whole bacterial cells: A review. Dyes Pigments, v. 58, 179-196 (2003).

Petzold, L. R., A description of DASSL: A differential/algebric equation system solver. STR-SAND 82-8637, Livermore (1982).

Rozada F., Calvo, L. F., García, A. I., Martín-Villacorta, J., Otero, M., Dye adsorption by sewage sludge-based activated carbons in batch and fixed-bed systems. Bioresource Technology, v. 87, 221-230 (2003).

Rozzi, A., Malpei, F., Bonomo, F., L., Bianchi, R., Textile wastewater reuse in northern Italy. Water Science Technology, v. 39, 121-128 (1999).

Ruthven, D. M., Principles of Adsorption and Adsorption Process. John Wiley & Sons, New York (1984).

Silva, E. A., Cossich, E. S., Tavares, C. R. G., Cardozo, L., Guirardello, R., Modeling of copper (II) biosorption by marine alga *Sargassum* sp. in fixed bed column. Process Biochemistry, v. 38, 791-799 (2002).

Thomas, H. C., Heterogeneous ion exchange in a flowing system. Journal of American Chemical Society, v. 66, 1664-1666 (1944).

Tütem, E., Apak, R., Ünal, Ç. F., Adsorptive removal of Chlorophenols from water by bituminous shale. Water Resources, v. 8(32), 2315-2324 (1998).

Valdman, E., Erijman, L., Pessoa, F. L. P., Leite, S. G. F., Continuous biosorption of Cu and Zn by immobilized waste biomass *Sargassum* sp. Process Biochemistry, v. 36, 869-873 (2001).